Published in final edited form as:
Invest Ophthalmol Vis Sci. 2009 April ; 50(4): 1515–1521. doi:10.1167/iovs.08-3010.

The aqueous humor outflow pathway of zebrafish

Matthew P. Gray[1,*], **Richard S. Smith**[2,*], **Kelly A. Soules**[1], **Simon W.M. John**[2,3,4], and **Brian A. Link**[1,¶]

[1]Department of Cell Biology and Anatomy, Medical College of Wisconsin, Milwaukee, WI 53226

[2]The Jackson Laboratory, Bar Harbor, ME 04609

[3]The Howard Hughes Medical Institute, Bar Harbor, ME 0409

[4]Department of Ophthalmology, Tufts University of Medicine, Boston, MA 02111

Abstract

PURPOSE—The structures of the ocular anterior segment responsible for aqueous humor secretion and absorption have been well characterized in mammals. However, the underlying molecular and cellular mechanisms that regulate flow have remained elusive. Experimental analysis in *Danio rerio*, the zebrafish, is providing mechanistic insights into many cellular processes relevant to normal human physiology and disease. To facilitate studies on the molecular and cellular mechanisms of aqueous humor dynamics using this species we have characterized the anatomy of aqueous secretion and outflow in adult zebrafish eyes.

METHODS—Analysis by light and transmission electron microscopy, coupled with molecular tracers of fluid flow, was employed to identify and study the sites of aqueous humor secretion and absorption in adult zebrafish eyes.

RESULTS—Zebrafish eyes show aqueous humor secretion primarily from the dorsal ciliary region and outflow through a ventral canalicular network that connects with an aqueous plexus and veins of the choroidal rete.

CONCLUSIONS—Vectorial flow of zebrafish aqueous humor is in contrast to mammals where secretion and absorption of aqueous humor is circumferential around and through the iridocorneal angle. However, local anatomy and ultrastructure of the tissues and cells specialized for aqueous humor dynamics in zebrafish shows conservation with that of mammals. These observations suggest that zebrafish can serve as a useful genetic model to help understand the regulation and cellular basis of normal and abnormal aqueous humor dynamics in humans.

INTRODUCTION

In the ocular anterior segment of vertebrates, production and outflow of aqueous humor is an important determinant of intraocular pressure and is required to maintain the proper shape and optical parameters of the eye. Aqueous humor flow also functions to circulate nutrients and to remove potentially harmful metabolites and cellular debris from the eye. In mammals, aqueous humor is produced circumferentially from the epithelia of ciliary processes. Mechanistically this is achieved by diffusion, ultrafiltration and active secretion of solutes and water [1–4]. The pigmented and non-pigmented ciliary epithelia function as a syncytium that transports and pumps ions and bioactive proteins into the anterior chamber [5, 6]. Water from ciliary body vasculature is then moved by osmotic forces across the epithelia and into

¶Correspondence to Brian A. Link: blink@mcw.edu.
*These authors contributed equally and are considered co-first authors

the posterior chamber. Aquaporins expressed by the ciliary epithelium can also directly transport water into the posterior chamber [7].

Aqueous humor then flows through the pupil into the anterior chamber and drains primarily through specialized structures at the iridocorneal angle, which are also organized circumferentially. Specifically, the humor filters through the trabecular meshwork and into Schlemm's canal. The trabecular meshwork is composed of an uveal layer of endothelial lined collagen- and elastin-rich trabecular beams that are covered by endothelial-like trabecular cells and a loose network of extracellular matrix referred to as the juxtacanalicular connective tissue [8–10]. The juxtacanalicular connective tissue has a complex organization with open areas filled with a glycoproteinacious extracellular matrix [11–15]. Aqueous humor percolates through the trabecular meshwork and ultimately traverses the inner wall endothelial cells of Schlemm's canal. Aqueous humor then flows from Schlemm's canal into collector channels of the episcleral venous system, which return the aqueous to the circulation. The major resistance for fluid drainage is generally thought to lie within the juxtacanalicular connective tissue and/or the inner wall of Schlemm's canal [16–21]. However, unlike production of aqueous humor, the molecular and cellular mechanisms of aqueous humor outflow remain debated and are not well understood. Understanding the mechanism of aqueous humor outflow has medical significance, as defects in outflow are the most common cause of elevated intraocular pressure [4].

Because elevated intraocular pressure is a major risk factor for the glaucomas, a group of progressive and blinding diseases of the optic nerve, we have characterized the anatomy associated with aqueous humor dynamics in zebrafish. The zebrafish experimental system has emerged as a power model for insights into the genetic basis and molecular and cellular mechanism of normal physiology and disease pathology. However, recent published observations suggest that the anterior segment anatomy of zebrafish varies from that of mammals [22–26]. In the current study, we use aqueous humor tracer experiments coupled with localized anatomical characterizations to investigate the aqueous humor outflow pathway of the zebrafish eye.

METHODS

Specimens

Wild-type zebrafish (*Danio rerio*) of the AB/AB and LF/LF backgrounds were reared under standard conditions with a light cycle of 14h light/10h dark. No differences in anterior segment anatomy were observed between these two strains. Specimens were collected between 9–14 months post fertilization. Prior to experimental manipulation or tissue fixation, fish were anesthetized in 0.2 mg per ml of ethyl 3-aminobenzoate methanesulfonate (tricane). All experiments were performed in compliance with the ARVO statement for use of animals in vision research.

Light Microscopy

Fish tissue was fixed in primary fixative [2% paraformaldehyde, 2.5% glutaraldehyde, 3% sucrose, 0.06% phosphate buffer (pH 7.4)] at 4°C for at least 18 hours. Tissue was washed in 0.1 M phosphate-buffered saline (PBS), dehydrated through an ethanol series and propylene oxide and then infiltrated with EMbed-812/Araldyte resin mixture. Transverse, semi-thin (1 μm), plastic sections were cut with a glass knife on a JB4 microtome. Serial sections were collected from near the central retina until the ventral canalicular network was first apparent as indicated by a break in the ventral iris pigmented epithelium. Following heat fixation to glass slides, sections were stained with 1% Toluidine Blue in 1% Borax buffer. Images were captured using a Nikon coolpix 995 digital color digital camera

mounted on a Nikon E800 compound microscope with a 60X oil-emersion objective. Serial sectioning through the ventral canalicular network was carried out on 10 eyes.

Transmission electron microscopy

TEM of fish eyes was carried out similarly to that described for the mouse (Smith et al., 2002). Fish were fixed in primary fixative and washed as for light microscopy. Specimens were then post-fixed with 1% Osmium Tetroxide on ice for 1 hour to preserve membranes. Tissue was dehydrated through a methanol series and acetonitrile and infiltrated with EMbed-812/Araldyte resin mixture. Ultrathin sections (60–70 nm) were collected on coated grids and stained with uranyl acetate and lead citrate for contrast. Images were captured using Hitachi H600 TEM. TEM was conducted on 6 eyes.

Ophthalmic artery injections

Fish were anesthetized as described above until they were unconscious and no longer responded to physical stimuli. Once anesthetized, a ~2 cm incision was made on the ventral surface of the fish superficial to the heart and gut. The fish were further dissected in order to expose the ophthalmic artery. The ophthalmic artery enters the dorsoposterior aspect of the eye parallel to the optic nerve. After exposing the ophthalmic artery, ~1.0 ul of lysine fixable 3kDa, biotinylated dextran (40mg/ml) (Molecular Probes of Invitrogen, D7135) was injected into the artery. The dextran solution was injected using a glass capillary pulled to a ~5 μm tip and delivered via a syringe driver. At either 2 or 10 minutes post injection, eyes were enucleated and fixed in 4% paraformeldehyde and subsequently processed for streptavidin-peroxidase binding and reactivity. For each time-point, 6 fish were assessed by ophthalmic artery tracer injections.

Intraocular Injections

Fish were anesthetized as described above until they were unconscious and no longer responded to physical stimuli. Once anesthetized, 500 nl of various aqueous humor tracers were injected into the anterior chamber over a period of 5 minutes in order to not damage anterior segment tissue and minimize pressure changes. The following molecular tracers were used in these experiments: (A) Lysine fixable 3kDa, rhodamine-conjugated dextran (40 mg/ml) (Molecular Probes of Invitrogen, D3308); (B) Purified type VI horse radish peroxidase (HRP, 25 mg/ml) (Sigma, P8375); (C) 10nm-gold-Bovine Serum Albumin (1:4 diluted stock with PBS) (EM Sciences, Cat#25486). The solutions were injected using a glass capillary pulled to a ~10 μm tip and delivered via a manual syringe driver. Epifluorescent microscopy was used to follow the dynamics of rhodamine-conjugated dextran in eyes from living, anesthetized specimens. For specimens injected with HRP, the heads of the fish were removed at prescribed intervals and fixed overnight in primary fixative. The heads were then bisected and prepared for peroxidase staining by incubating the tissue in 0.5 mg/ml 3,3′-diaminobenzidine + 0.003% H_2O_2 buffered in PBS [27]. These eyes, as well as those injected with 10nm-gold-Bovine Serum Albumin were further processed for TEM as described above. For each experiment, at least 6 eyes were assessed.

RESULTS

Several feature of the zebrafish eye suggest a unique system for aqueous humor circulation (Figure 1A, Figure 5). Unlike mammals, the zebrafish eye lacks ciliary processes and a circumferential organization of trabecular meshwork and ouflow channels. Instead, circumferential at the iridocorneal angle of teleosts is a hypertrophied-appearing structure called the annular ligament [23, 25, 26, 28, 29]. A recent study has suggested the annular ligament of zebrafish is equivalent to the mammalian trabecular meshwork [26]. While the morphology of the annular ligament differs significantly with that of mammalian

iridocorneal angle specialization, the circumferential nature and location of this structure is consistent with this notion. However, experimental analysis presented below indicates this in not the case.

Previous studies of the developing anterior segment of zebrafish showed that the dorsal ciliary epithelium, despite lacking processes, appears specialized for aqueous humor secretion [23]. At the ventral iridocorneal angle, a focal canalicular network was found suggestive of an aqueous outflow pathway. In adult zebrafish, we find that these dorsal and ventral features are maintained. Ultrastructurally, the dorsal ciliary epithelium is composed of apical-apical facing pigmented and non-pigmented cells coupled by adherens and tight junctions (Figure 1B). The non-pigmented epithelium shows numerous vesicles and intracellular membranous infoldings, similar to that of mammalian secretory ciliary epithelium [5, 27]. By light microscopy the anterior portion of the ventral canalicular network (the iridocorneal canal) appears as an endothelium separating the argentea and stroma of the iris from the annular ligament (Figure 1C). The posterior portion of the ventral canalicular network (the ciliary canal) is distinguished by a break between the retinal pigment epithelium and the pigmented ciliary epithelium. The ciliary part of the canalicular network, as well as parts of the angular aqueous plexus fill the space between the breaks in the pigmented epithelia (Figure 1C, D). After fixation, the angular aqueous plexus is often filled with blood cells. Also by light microscopy, this region of the ventral angle is noted by the presence of thumb-like structure underlying and associated with the ventral iris (Figure 1C). In other species of fish and amphibians, this structure is called the retractor lentis – a muscular tissue that functions to move the lens during accommodation [28]. However, in zebrafish the retractor lentis may be vestigal as there is no evidence for lens accommodation in this species [30].

To investigate the finer morphology of the ventral canalicular network we analyzed this region by transmission electron microscopy (TEM). We found the canalicular network is lined by an endothelium 2–4 cells thick. The endothelial cells lining the canals and openings show numerous clatherin coated pits and endocytic vesicles (Figure 1F, G). Overall, the endothelium is highly complex in organization such that thin sections give a “topographical map” appearance owing to the plasma membranes of the interdigitating cells (Figure 1H). Electron dense junctional complexes couple the interdigitated endothelial cells (Figure 1H, I). At the opening of the canalicular network at both the ciliary and iridocorneal regions a loosely organized juxtacanalicular connective tissue exists (Figure 1D, J). A tortuous canalicular network formed by the spaces between endothelial cells can be traced from the iridocorneal angle to the angular aqueous plexus that resides between the ventral scleral ossicle and rim of the neural retina (Figure J–M). Serial sectioning indicated that the width of the canalicular network was typically less than 75 microns. Endothelial cells lining the opening of the canalicular network at both the ciliary region and iridocorneal angle, as well as endothelial cells adjacent to the angular aqueous plexus at the termination of the canalicular network, show parachuting morphologies and giant vacuoles. Their morphologies are similar to those of mammalian endothelial cells lining Schlemm’s canal and arachnoid cells lining the ventricles of the central nervous system [31, 32] (Figure 1M). TEM also revealed the angular aqueous plexus is continuous with vessels of the choroidal rete. Cumulative, this anatomy suggests this region as the outflow pathway for aqueous humor in zebrafish.

To more directly investigate the routes of aqueous humor movement in zebrafish we injected 3kDa biotinylated dextrans into the ophthalmic artery of living, anesthetized zebrafish and fixed these specimens after 2 or 10 minutes post injection. The ophthalmic artery directly feeds the ciliary vessels that supply aqueous humor in mammals and this sized dextran is small enough to be secreted with aqueous humor [27336]. Following injections into the

ophthalmic artery, eyes were enucleated and processed as whole tissues for the location of the 3kDa dextran using streptavidin coupled to Horse Radish Peroxidase (HRP). In the presence of 3,3′-diaminobenzidine, HRP produces a reddish-brown precipitate. Within 2 minutes after injections into the ophthalmic artery, 3kDa dextran could be detected throughout the anterior chamber, with enrichment in both the dorsal and ventral regions of the eye (Figure 2A). By 10 minutes following a single bolus injection, HRP reactivity was found only in the ventral quadrant or the eye, with most intense staining at the opening of the ventral canalicular network (Figure 2B). These data are consistent with morphological findings suggesting that aqueous humor is produced in the dorsal hemisphere and leaves the anterior segment of the eye via the ventral canalicular network.

In a related set of experiments we injected 3kDa rhodamine conjugated dextan directly into the ocular anterior segments of anesthetized zebrafish and observed the movement of this tracer by fluorescence microscopy (Figure 2C,D). To minimize changes in IOP induced by fluid injection, 100 nl per minute of the10kDa dextran solution was delivered with a manual syringe driver over a period of 5 minutes. Anesthetized zebrafish rested horizontally throughout the experiment, so that gravitational forces could not bias the movement of tracer to either the dorsal or ventral pole. Immediately following the start of the injection fluorescence was found throughout the anterior segment (Figure 2E). Within 15 minutes following the injection, the majority of dextran was found ventrally and in association with the ventral canalicular network (Figure 2F). Evidence of rhodamine-dextran in the vasculature throughout the fish was also apparent. At 15 minutes the eyes were enucleated and fluorescence was found in the ventral choroidal rete at the back of the eye (Figure 2G–I). A subset of these eyes were fixed and further processed for histological sections. Endothelial cells of the ventral canalicular network showed strong fluorescence (Figure J,K). No fluorescence was found in the annular ligament. In addition, very little fluorescence was found within the aqueous plexus suggesting that once the dextrans were delivered to this sinus, they were rapidly swept away by blood flow.

In a final set of experiments, we injected additional tracers into the anterior segment that could be coupled with TEM to better inspect the cellular fate and movement of aqueous humor. We gently injected 10nm gold conjugated to Bovine Serum Albumin protein (10nm-gold-BSA) into the anterior chamber over the course of 5 minutes. In the first experiments, the eyes of anesthetized zebrafish were removed and fixed for TEM ten minutes after the start of the 5-minute anterior segment injection. Ultrastructural analysis revealed the presence of 10nm-gold-BSA throughout the ventral canalicular network, but not within the annular ligament (Figure 3). The electron dense tracer was also found to be endocytosed by ventral canalicular endothelial cells (Figure 2B, C). A small amount of 10nm-gold-BSA was also found in the angular aqueous plexus in association with inner wall endothelial cells (Figure 3E–G). In subsequent experiments, we similarly injected purified HRP and fixed eyes immediately following the 5-minute injection. Eyes were then processed for HRP reactivity and TEM. Consistent with our previous results, we found HRP associated with the surface of the annular ligament, but it had not entered into the tissue (Figure 4B). HRP reactivity was also associated with the posterior iris epithelium, but was not found in the cells or in the iris stroma (Figure 4C). HRP reactivity was found in the angular aqueous plexus in what appeared as a gradient with the highest concentrations closest to the anterior chamber (Figure 4D). Surprisingly, we also found HRP reactivity in association with endothelial cells of ventral vitreal-retinal vessels and also within the vessel lumens (Figure 4E). These vessels line the interface of the vitreal-retinal boundary and show a higher density in the ventral portion of the eye [24]. No HRP reactivity, however, was found in the dorsal vitreal-retinal vessels.

DISCUSSION

Using light and electron microscopy with molecular tracers of aqueous humor movement, we have described the aqueous humor drainage pathway of zebrafish. Our data support a model where aqueous humor is produced in the dorsal hemisphere by the ciliary epithelium and removed via a ventral canalicular network that connects to the angular aqueous plexus (Figure 5). This plexus is continuous with the choroidal venous system where aqueous humor returns to the vascular circulation. Aqueous humor also appears to be taken up by ventrally localized vitreal-retinal vessels. We did not find evidence of uveal-scleral outflow, although our techniques and timing of tracer experiments were not designed to evaluate this potential secondary route of aqueous outflow.

Despite the unique vectoral flow of aqueous humor of zebrafish, local anatomical features and cellular ultrastructure of this system has similarities to the aqueous humor pathway of mammals. Similarities include the morphology of juxtacanalicular tissue overlying the outflow pathway and the morphology and organization of the endothelial cells that line the canalicular network. In particular the endothelial cells show a high degree of junctional coupling and complex cell shapes and intracellular interactions. The canalicular endothelial cells of zebrafish are also highly phagocytic, like the endothelial cells associated with Schlemm's canal in mammals [9; 34]. In addition, a sub-set of these cells displayed distended or parachuting morphologies. The distended morphologies, resembling giant vacuoles, were most frequent in cells lining the entrance and exit of the canalicular network proximal to the anterior chamber and ventral angular aqueous plexus, respectively. A noted difference with mammals is an absence of obvious trabecular beams. Although other investigators have suggested that the annular ligament of zebrafish represents the trabecular meshwork equivalent [26], we view this structure as distinct and unique. Instead we suggest the cells overlying the ventral canalicular network at both the iridocorneal and ciliary openings are homologous to the juxtacanalicular connective tissue cells of the mammalian trabelcular meshwork and by extension, the canalicular network is homologous to Schlemm's canal.

Like anatomical and tracer experiments in mammals, our studies have not addressed the molecular and cellular mechanisms that facilitate and regulate aqueous humor outflow. In mammals, paracellular and transcellular routes of fluid movement through angle endothelial cells have been proposed [34]. The results from the anatomy and tracer experiments from zebrafish are also consistent with either or both mechanisms. Our studies also suggest that like mammals, the point of major resistance of aqueous humor movement is located at the opening of the canalicular outflow pathway. Importantly, the description of homologous aqueous humor outflow tissues in zebrafish provide the opportunity for genetic studies to probe the specific molecular and cellular mechanisms that control aqueous humor dynamics and intraocular pressure.

Acknowledgments

We thank Olga Savinova and Michael Cliff for assistance with sectioning and animal husbandry, Clive Wells for assistance with TEM, and Xinping Zhao for helpful discussions and sharing unpublished data that confirmed some of our studies. We also gratefully acknowledge the following funding support: Howard Hughes Medical Institute (SWMJ), Pilot funds from The Glaucoma Foundation (BAL), NIH R01EY16060 (BAL), and NEI Core Facilities grant P30EY001931 to the vision research community of MCW.

References

1. Cole DF. Transport across the Isolated Ciliary Body of Ox and Rabbit. Br J Ophthalmol. 1962; 46(10):577–91. [PubMed: 18170817]

2. Green K, Pederson JE. Aqueous humor formation. Exp Eye Res. 1973; 16(4):273–86. [PubMed: 4741254]
3. Pederson JE, Green K. Aqueous humor dynamics: experimental studies. Exp Eye Res. 1973; 15(3): 277–97. [PubMed: 4695439]
4. Gabelt, BT.; Kaufman, PL. Aqueous humor hydrodynamics. 10. St. Louis, MO: Mosby; 1997.
5. Raviola G, Raviola E. Intercellular junctions in the ciliary epithelium. Invest Ophthalmol Vis Sci. 1978; 17(10):958–81. [PubMed: 100466]
6. Coca-Prados M, Escribano J. New perspectives in aqueous humor secretion and in glaucoma: the ciliary body as a multifunctional neuroendocrine gland. Prog Retin Eye Res. 2007; 26(3):239–62. [PubMed: 17321191]
7. Zhang D, Vetrivel L, Verkman AS. Aquaporin deletion in mice reduces intraocular pressure and aqueous fluid production. J Gen Physiol. 2002; 119(6):561–9. [PubMed: 12034763]
8. Ashton N. The exit pathway of the aqueous. Trans Ophthalmol Soc UK. 1960; (80):397.
9. Tripathi RC. Ultrastructure of the exit pathway of the aqueous in lower mammals (A preliminary report on the “angular aqueous plexus”). Exp Eye Res. 1971; 12(3):311–4. [PubMed: 5130275]
10. Gong HY, Trinkaus-Randall V, Freddo TF. Ultrastructural immunocytochemical localization of elastin in normal human trabecular meshwork. Curr Eye Res. 1989; 8(10):1071–82. [PubMed: 2612196]
11. Bhatt K, Gong H, Freddo TF. Freeze-fracture studies of interendothelial junctions in the angle of the human eye. Invest Ophthalmol Vis Sci. 1995; 36(7):1379–89. [PubMed: 7775116]
12. Lutjen-Drecoll E, Shimizu T, Rohrbach M, Rohen JW. Quantitative analysis of ‘plaque material’ in the inner- and outer wall of Schlemm’s canal in normal- and glaucomatous eyes. Exp Eye Res. 1986; 42(5):443–55. [PubMed: 3720863]
13. Gong H, Ruberti J, Overby D, Johnson M, Freddo TF. A new view of the human trabecular meshwork using quick-freeze, deep-etch electron microscopy. Exp Eye Res. 2002; 75(3):347–58. [PubMed: 12384097]
14. Smith RS, Zabaleta A, Savinova OV, John SW. The mouse anterior chamber angle and trabecular meshwork develop without cell death. BMC Dev Biol. 2001; 1(1):3. [PubMed: 11228591]
15. Acott TS, Kelley MJ. Extracellular matrix in the trabecular meshwork. Exp Eye Res. 2008; 86(4): 543–61. [PubMed: 18313051]
16. Grierson I, Lee WR. Pressure effects on flow channels in the lining endothelium of Schlemm’s canal. A quantitative study by transmission electron microscopy. Acta Ophthalmol (Copenh). 1978; 56(6):935–52. [PubMed: 103360]
17. Ethier CR, Kamm RD, Palaszewski BA, Johnson MC, Richardson TM. Calculations of flow resistance in the juxtacanalicular meshwork. Invest Ophthalmol Vis Sci. 1986; 27(12):1741–50. [PubMed: 3793404]
18. Brilakis HS, Johnson DH. Giant vacuole survival time and implications for aqueous humor outflow. J Glaucoma. 2001; 10(4):277–83. [PubMed: 11558811]
19. Johnson M, Shapiro A, Ethier CR, Kamm RD. Modulation of outflow resistance by the pores of the inner wall endothelium. Invest Ophthalmol Vis Sci. 1992; 33(5):1670–5. [PubMed: 1559767]
20. Maepea O, Bill A. Pressures in the juxtacanalicular tissue and Schlemm’s canal in monkeys. Exp Eye Res. 1992; 54(6):879–83. [PubMed: 1521580]
21. Johnson M. What controls aqueous humour outflow resistance? Exp Eye Res. 2006; 82(4):545–57. [PubMed: 16386733]
22. Kanungo J, Swamynathan SK, Piatigorsky J. Abundant corneal gelsolin in Zebrafish and the ‘four-eyed’ fish, Anableps anableps: possible analogy with multifunctional lens crystallins. Exp Eye Res. 2004; 79(6):949–56. [PubMed: 15642334]
23. Soules K, Link B. Morphogenesis of the anterior segment in the zebrafish eye. BMC Dev Biol. 2005; 5:12. [PubMed: 15985175]
24. Alvarez Y, Cederlund ML, Cottell DC, et al. Genetic determinants of hyaloid and retinal vasculature in zebrafish. BMC Dev Biol. 2007; 7:114. [PubMed: 17937808]

25. Yoshikawa S, Norcom E, Nakamura H, Yee RW, Zhao XC. Transgenic analysis of the anterior eye-specific enhancers of the zebrafish gelsolin-like 1 (gsnl1) gene. Dev Dyn. 2007; 236(7):1929–38. [PubMed: 17576137]
26. Chen CC, Yeh LK, Liu CY, et al. Morphological differences between the trabecular meshworks of zebrafish and mammals. Curr Eye Res. 2008; 33(1):59–72. [PubMed: 18214743]
27. Smith RS. Ultrastructural studies of the blood-aqueous barrier. 1: Transport of an electron-dense tracer in the iris and ciliary body of the mouse. Americal Journal of Ophthalmology. 1971; 71(5): 1066–77.
28. Walls, GL. The vertebrate eye and its adaptive radiation. New York, New York: Hafner Publishing Company; 1942.
29. Tripathi, RC. Comparative physiology and anatomy of the outflow pathway. New York, New York: Academic Press; 1974.
30. Easter SS Jr, Nicola GN. The development of vision in the zebrafish (Danio rerio). Dev Biol. 1996; 180(2):646–63. [PubMed: 8954734]
31. Tripathi RC. Microcirculation of the aqueous humour: ultrastructural study of the outflow mechanism. J Pathol. 1971; 103(2):P8. [PubMed: 5567930]
32. Alksne JF, Lovings ET. Functional ultrastructure of the arachnoid villus. Arch Neurol. 1972; 27(5):371–7. [PubMed: 5078893]
33. Smith RS, Rudt LA. Ultrastructural studies of the blood-aqueous barrier. 2. The barrier to horseradish peroxidase in primates. Am J Ophthalmol. 1973; 76(6):937–47. [PubMed: 4202452]
34. Epstein DL, Rohen JW. Morphology of the trabecular meshwork and inner-wall endothelium after cationized ferritin perfusion in the monkey eye. Invest Ophthalmol Vis Sci. 1991; 32(1):160–71. [PubMed: 1987099]

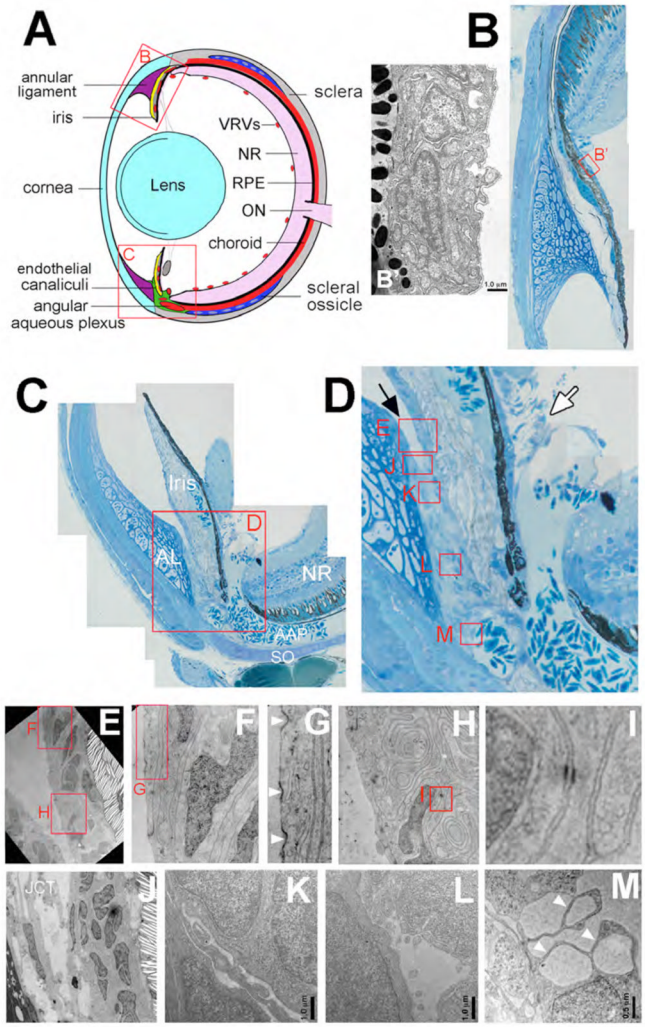

Figure 1.

Anatomy of the iridocorneal angles of adult zebrafish. (A) Schematic of tissues in the adult zebrafish eye. In all panels dorsal is up, ventral is down, anterior is left and posterior is right. (B) Toluidine -blue stained semi-thin section montage of a dorsal iridocorneal angle. (B′). High magnification TEM inset of pigmented and non-pigmented epithelia of the dorsal ciliary region. (C) Semi-thin section montage of a ventral iridocorneal angle. (D) Higher magnification of endothelial canalicular tissue and adjacent structures indicating area for TEM analysis (red boxed regions). Iridocorneal canal opening indicated with black arrow; ciliary canal opening indicated with white arrow (E–I) High magnification TEM inset of cells in the ventral canalicular network. Note the numerous coated pits and micropinocytic vesicles in G (white arrowheads), and the tight and adherens junctions between endothelial cells in H and I. (J–M) TEM of canalicular endothelia and openings. Note the loosely organized juxtacanalicular connective tissue (JCT) at the opening of the canaliculi in J and the parachuting morphology and giant vacuoles of endothelial cells adjacent to the angular aqueous plexus in M (white arrowheads). Scale bars equal 1.0 μm in B′, K, L and 0.5 μm in M. VRVs, vitreal-retinal vessels (red); NR, neural retina (pink); RPE, retinal pigment epithelium (black); ON, optic nerve (pink); sclera (grey); SO, scleral ossicle (dark blue); AAP, angular aqueous plexus (red); endothelial canaliculi (green); cornea and lens (light blue); annular ligament (purple).

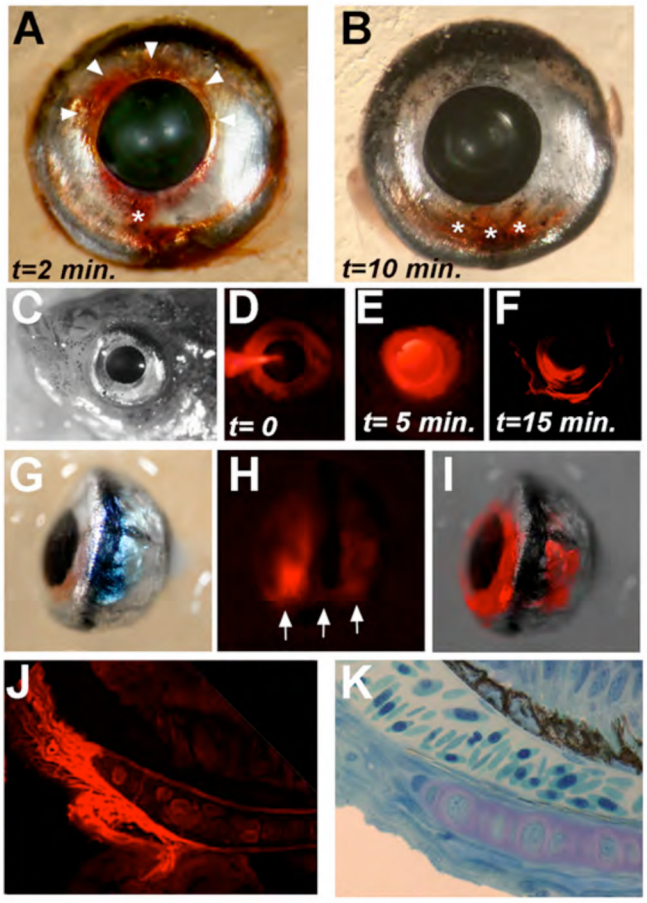

Figure 2.

Tissue fate of aqueous humor tracers in zebrafish eyes. (A–B) Peroxidase staining to localize secretion and absorption of 3kDa biotin-dextrans that were injected into the ophthalmic artery. Eyes were enucleated and fixed after (A) 2 minutes or (B) 10 minutes. Note the dorsally localized peroxidase product in A (white arrowheads) and the ventrally localized staining in both A and particulary B (white asterisks). (C) Brightfield microscopy of anesthetized zebrafish eye prior to anterior segement injection of 3kDa rhodamine-dextran. (D–F) Fluorescence microscopy of anesthetized zebrafish eye during (D) and 5 minutes (E) and 15 minutes (F) after anterior segement injection of 3kDa rhodamine-dextran. (G–H) Ventral view of isolated eyes following anterior segement injection of 3kDa rhodamine-dextran showing brightfield microscopy (G), fluorescence microscopy (H), and overlayed images. Note the concentrated fluorescence in the ventral iridocorneal angle and choroidal tissues (white arrows). (J) Fluorescence microscopy of semi-thin section of ventral endothelial canaliculi following anterior segement injection of 3kDa rhodamine-dextran. (K) Brightfield microscopy of equivalent section to J stained with Toluidine blue to highlight the relative locations of the endothelial canaliculi, angular aqueous plexus, scleral ossicle, and neural retina.

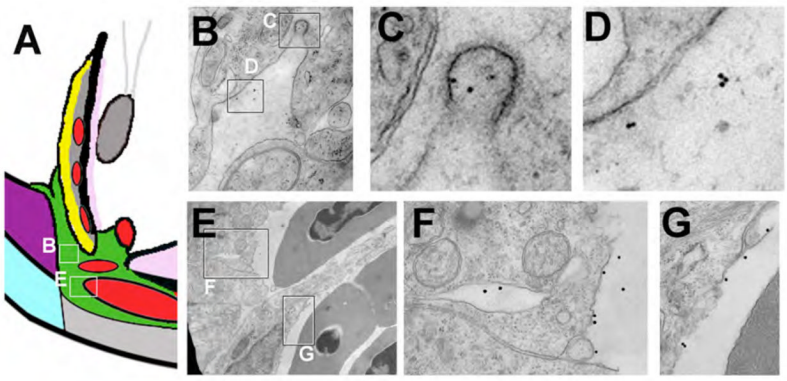

Figure 3.

Movement of 10nm-gold-BSA through the ventral canalicular network. (A) Schematic of the ventral angle to indicate locations of TEM images. Following injection of 10nm-gold-BSA into the anterior chamber, zebrafish eyes were fixed and processed for TEM. (B–D) TEM showing electron dense 10nm-gold-BSA localized to coated endocytic pits of canalicular endothelial cells (C) and within open spaces between endothelial cells (D). (E–G) TEM of endothelial cells lining the ventral angular aqueous plexus and highlighting 10nm-gold-BSA at the termination of the outflow pathway.

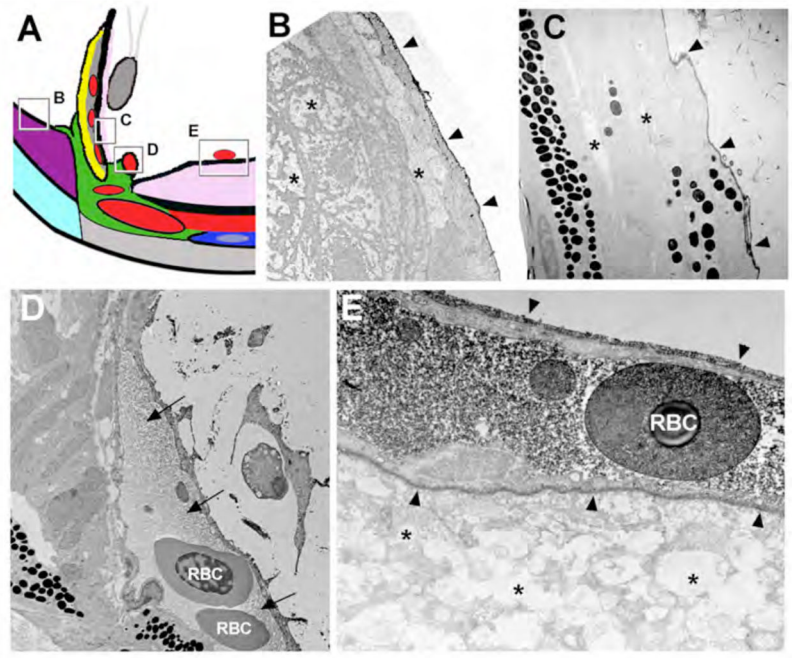

Figure 4.

Peroxidase activity following HRP injection in the anterior chamber. (A) Schematic of the ventral angle to indicate locations of TEM images. (B) Dark appearing peroxidase activity is associated with the epithelium covering the annular ligament (arrowheads), but is not found within or between annular ligament cells (asterisks). (C) Similarly, peroxidase activity is associated with the non-pigmented epithelial surface of the iris (arrowheads), but not within or between epithelial or stromal cells (asterisks). (D) A sinus of the angular aqueous plexus showing peroxidase activity (fluid surrounding the RBCs, arrows). (E) Peroxidase staining associated with endothelial cells (arrowheads) and within the lumen of vitreal-retinal vessels (fluid surrounding the RBC). No staining was noted in the nerve fiber layer of the neural retina (asterisks). RBC, red blood cell.

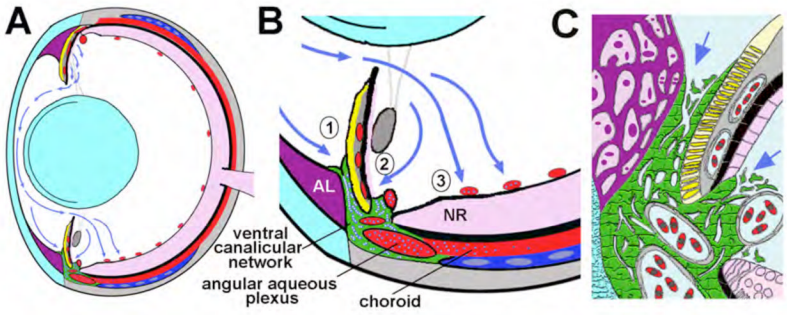

Figure 5.

Model of aqueous humor dynamics in the zebrafish eye. (A) Overview showing the vectorial flow of aqueous humor (blue arrows) from the dorsal ciliary epithelium to the ventral canalicular network and ventral vitreal-retinal vessels. (B) Higher magnification of aqueous humor outflow indicating absorption into (1) the iridocorneal and (2) ciliary openings of the ventral canalicular network and (3) ventral vitreal-retinal vessels. (C) Higher detail of the outflow pathway showing juxtacanalicular connective tissue cells at the iridocorneal and ciliary openings (indicated by arrows) and the tortuous lacunae created by endothelial cells (green) lining the canalicular network – for comparison see Figure 1D. Lens and cornea, light blue; annular ligament (AL), purple; blood-filled vessels and sinuses, red; iris argentea, yellow; iris stroma, lentis retractor, and sclera, grey; neural retina (NR), pink; scleral ossicle, dark blue; aqueous humor in outflow tissues, blue-white dots in A and B and pale blue in C.